JOURNAL OF MOLECULAR SPECTROSCOPY **179,** 334–341 (1996)
ARTICLE NO. 0212

REMPI Spectra of Cl_2: Vibrational and Rotational Analysis of the $2^1\Pi_g$ Rydberg States of $^{35}Cl_2$, $^{35}Cl^{37}Cl$, and $^{37}Cl_2$

Gísli Hólmar Jóhannesson, Huasheng Wang, and Ágúst Kvaran

Science Institute, University of Iceland, Dunhaga 3, 107 Reykjavík, Iceland

Received March 15, 1996; in revised form May 8, 1996

Rotational contours of the (2 + 1) resonance enhanced multiphoton ionization (REMPI) spectra of the vibrational bands corresponding to the $2^1\Pi_g \leftarrow X$ transitions in $^{35}Cl_2$, $^{35}Cl^{37}Cl$, and $^{37}Cl_2$ for the natural abundance of isotopes have been recorded at room temperature. Vibrational bands consist of contributions from all three isotopomers with varying degrees of overlap depending on vibrational quantum numbers. Band heads and tails were analyzed by simulation calculation. Rotational constants ($B_{v'}$ and $D_{v'}$) and corresponding internuclear distances ($r_{v'}$) for the Rydberg state were obtained, as well as equilibrium position rotational parameters. Thus for $^{35}Cl_2$, $B'_e = 0.2763 \pm 0.0008$ cm^{-1}, $\alpha'_e = 0.0015 \pm 0.0001$ cm^{-1}, and $r'_e = 1.868 \pm 0.005$ Å. Vibrational analyses based on the determination of band origins from the spectral simulations were performed to obtain $\omega'_e = 664.8 \pm 0.2$ cm^{-1}, $\omega_e x_e = 2.62 \pm 0.02$ cm^{-1} for $^{35}Cl_2$, and $T'_e = 63970 \pm 3$ cm^{-1}. Spectroscopic parameters for $^{35}Cl^{37}Cl$ and $^{37}Cl_2$ are derived from those for $^{35}Cl_2$ in a standard way (see text).

INTRODUCTION

Electronically highly excited states of molecular chlorine have received considerable attention experimentally recently (*1–15*). These have mainly been detected and analyzed by one-photon vacuum ultraviolet (VUV) absorption and fluorescence spectroscopy (*4, 5, 7, 11, 14*), by optical–optical double resonance spectroscopy (*1, 6, 15*), or by resonance-enhanced multiphoton ionization techniques (*1–5, 7–10, 12, 13*) (REMPI). Analysis of the experimental data has largely benefited from ab initio calculations made by Peyerimhoff and Buenker (*16*). These extensive quantum-chemical calculations, which include configuration interaction, but neglect spin–orbit coupling, reveal several avoided crossings between Rydberg and valence states, which give rise to adiabatic double-well potential energy curves. Experimental studies of the excited states of chlorine can be divided into those of the ungerade states which are accessed by an odd number of photon excitations from the gerade ground state ($X\,^1\Sigma_g^+$) (*3–5, 7, 9, 11, 12, 14*) and those of the gerade states which can be accessed with an even number of photon excitations (*1, 2, 6, 8, 10, 13, 15*). Furthermore, the states observed are either Rydberg states (*1, 2, 8–10, 12–14*) or ion-pair states (*1–3, 6, 15*) or a mixture of both due to homogeneous interactions (*4, 5, 7, 9–12*). Most of the spectroscopic studies have been low- or medium-resolution work emphasizing vibrational analysis. More explicit assignments and analysis of the excited states by virtue of rotational analyses of vibrational bands have been made only to a limited extent (*5, 8, 17*).

The lowest energy Rydberg states, $2^1\Pi_g$ and $2^3\Pi_g$, corresponding to $4s \leftarrow \pi_g$ transitions, have been studied by (2 + 1) REMPI, combined with ion mass detection (*1, 10, 13*) and kinetic energy resolved electron detection (*8*). Both states have been predicted to mix homogeneously with ion-pair states to form adiabatic double-well potentials (*16*). Inner well levels from $v' = 0$ to $v' = 19$ have been observed for $2^1\Pi_g$, showing virtually unperturbed Rydberg character (*1, 8*), while inner well levels for $2^3\Pi_g$ have been observed from $v' = 0$ to the top of the double-well barrier, and well beyond that to levels spanning both wells. Observation of these long progressions has been attributed to excitation via a repulsive continuum at a one-photon level (*1, 10*). Furthermore, photoelectron spectra data for the $2^1\Pi_g$ state have been interpreted in terms of a competition between electronic autoionization and dissociation from Rydberg states followed by atom ionization in the final ionization steps (*8*).

In this paper we present measurements and analyses of (2 + 1) REMPI vibrational bandheads and rotational contours corresponding to transitions to the $2^1\Pi_g$ (alternative expression: $[^2\Pi_{1/2g}]_c 4s;\ 1g$) Rydberg state for the isotopomers $^{35}Cl^{35}Cl$ (i.e., $^{35}Cl_2$), $^{35}Cl^{37}Cl$, and $^{37}Cl^{37}Cl$ (i.e., $^{37}Cl_2$) at room temperature. The vibrational bands in the spectra are interpreted and analyzed by spectral simulations to derive precise rotational and vibrational parameters for the Rydberg state.

EXPERIMENTAL DETAILS

The apparatus used has been described in detail elsewhere (*18, 19*), so only a brief report will be given here. Tunable laser pulses were generated using a Lumonics Hyperdye 300 laser pumped by a Lumonics 510 excimer laser. The

0022-2852/96 $18.00

wavelength range studied, 272–313 nm, was covered by using the frequency-doubled output from the dyes Rhodamine 610, Rhodamine 590, and Coumarine 540A. The frequency-doubled beam was separated from the fundamental beam by means of a Pellin Broca prism. A 10-cm focal-length lens was used to focus the pulses from the dye laser into an ionization glass cell fitted with stainless steel electrodes (15 mm diameter and about 20 mm apart). The electrodes were typically kept at ±250 V by batteries. The cell usually contained molecular chlorine vapor at 0.5–1.0 Torr pressure (Merck, 99.8%) at room temperature. Current pulses were amplified by a balanced bias differential amplifier, integrated, and fed into a multichannel analyzer for voltage peak height detection and recording. Average pulse heights for a fixed sampling time were recorded and displayed as a function of the two-photon wavenumber ($\bar{\nu}_{2h\nu}$) by an IBM/XT computer.

The laser was run at 20 Hz repetition rates for sampling times of 5–120 sec. The bandwidth of the laser beam from the dye laser was about 0.05 cm^{-1}. The dye laser output was scanned in 1.0–2.0 cm^{-1} steps for low-resolution spectra but in 0.1–0.2 cm^{-1} steps for high-resolution spectra. The laser power was kept as low as possible in order to prevent power broadening. Calibration of the wavelength was achieved by recording the neon signal from an optogalvanic cell (visible region) and the REMPI signal from iodine atomic lines (UV region) (*20*). The accuracy of the calibration, as judged from the position of the atomic lines in the spectral region studied here, was found to be ±2 cm^{-1} on the two-photon wavenumber scale.

RESULTS AND DATA ANALYSIS

(a) REMPI Spectra: Interpretations

The rotational contour for the (2, 0) band in the $2^1\Pi_g \leftarrow X$ system is shown in Fig. 1a plotted on a two-photon wavenumber scale ($\bar{\nu}_{2h\nu}$ [cm^{-1}]). Bandheads of the vibrational bands (v', v'') = (2, 0), (5, 0), (6, 0), and (9, 0) are shown in Fig. 1b. Bands (0, 0) and (8, 0) were partly resolved, while other vibrational bands in the system showed broad unresolved structure, were overlapped by some unidentified peaks, or were too weak to be detected.

The vibrational bands consist of overlapping bands due to the isotopomers $^{35}Cl_2$ (characterized by 35 from now on), $^{35}Cl^{37}Cl$ (35/37), and $^{37}Cl_2$ (37) in their natural abundances. The band origin ($\bar{\nu}^0(i; v', v'')$) of a vibrational band (v', v'') corresponding to isotopomer i (i = 35, 35/37, 37) is determined by

$$\bar{\nu}^0(i; v', v'') = T'_e + \{\omega'_e(i)(v' + \tfrac{1}{2}) - \omega_e x'_e(i)(v' + \tfrac{1}{2})^2\} - \{\omega''_e(i)(v'' + \tfrac{1}{2}) - \omega_e x''_e(i)(v'' + \tfrac{1}{2})^2\}, \quad [1]$$

where $\omega'_e(i)$ and $\omega''_e(i)$ are the vibrational frequencies for the Rydberg state and the ground state, respectively, and $\omega_e x'_e(i)$ and $\omega_e x''_e(i)$ are the corresponding anharmonicity constants. T'_e is the electronic energy minimum for the Rydberg states potential. The relationship between the vibrational constants and the anharmonicity constants for different isotopomers (i and j), based on the ratio of the reduced masses ($\rho(i, j)^2$), is

$$\omega_e(i) = \omega_e(j)\rho(i, j) \quad [2]$$

$$\omega_e x_e(i) = \omega_e x_e(j)\rho^2(i, j), \quad [3]$$

where

$$\rho(i, j) = \sqrt{\frac{\mu_j}{\mu_i}} \quad [4]$$

and μ_i and μ_j are the reduced masses of the corresponding isotopomers i and j. Given Eqs. [1]–[4] one can evaluate the spacing between the band origins of different isotopomers for the same (v', v'') (isotope shift), $\Delta\bar{\nu}^0(i, j) = \bar{\nu}^0(i; v', v'') - \bar{\nu}^0(j; v', v'')$, by

$$\Delta\bar{\nu}^0(i, j) = [\omega'_e(i)(v' + \tfrac{1}{2}) - \omega''_e(i)(v'' + \tfrac{1}{2})] \times [1 - \rho(i, j)] - [\omega_e x'_e(i)(v' + \tfrac{1}{2})^2 - \omega_e x''_e(i)(v'' + \tfrac{1}{2})^2][1 - \rho^2(i, j)] \quad [5]$$

$$\approx [\omega'_e(i)(v' + \tfrac{1}{2}) - \omega''_e(i)(v'' + \tfrac{1}{2})][1 - \rho(i, j)] \quad [6]$$

for small v' and v''. For the halogens and the interhalogens ω'_e is usually larger than ω''_e (*19–21*), and since $\rho(35, 35/37) < 1$ and $\rho(35/37, 37) < 1$, $\Delta\bar{\nu}^0(35, 35/37) > 0$ and $\Delta\bar{\nu}^0(35/37, 37) > 0$ for (v'', 0) bands. Thus the relative positions of the band origins are

$$\bar{\nu}^0(35) > \bar{\nu}^0(35/37) > \bar{\nu}^0(37) \quad [7]$$

as indicated on Fig. 1a for the (2, 0) band. Furthermore, since the natural abundance of atomic chlorine is 24.23% (^{37}Cl) and 75.77% (^{35}Cl), the natural abundance of molecular chlorine, hence the relative intensity, is 57.41% ($^{35}Cl_2$), 36.72% ($^{35}Cl^{37}Cl$), and 5.87% ($^{37}Cl_2$).

Each bandhead of a particular isotopomer consists of two sharp peaks, the *O* peak and the *P* peak, due to overlap of rotational lines in the *O*-line series and the *P*-line series, respectively (*18, 19, 21*). The relative intensities of the *O* and *P* peaks are consistent with $\Delta\Omega = 1$ transitions, confirming the $2^1\Pi_g$ assignment of the Rydberg state (*22, 23*). The peaks in the bandheads in Fig. 1b are labeled with O_{35}, P_{35}, $O_{35/37}$, $P_{35/37}$, O_{37}, and P_{37}. In the figure the bands are normalized to the position of O_{35}. The absolute *O*-peak

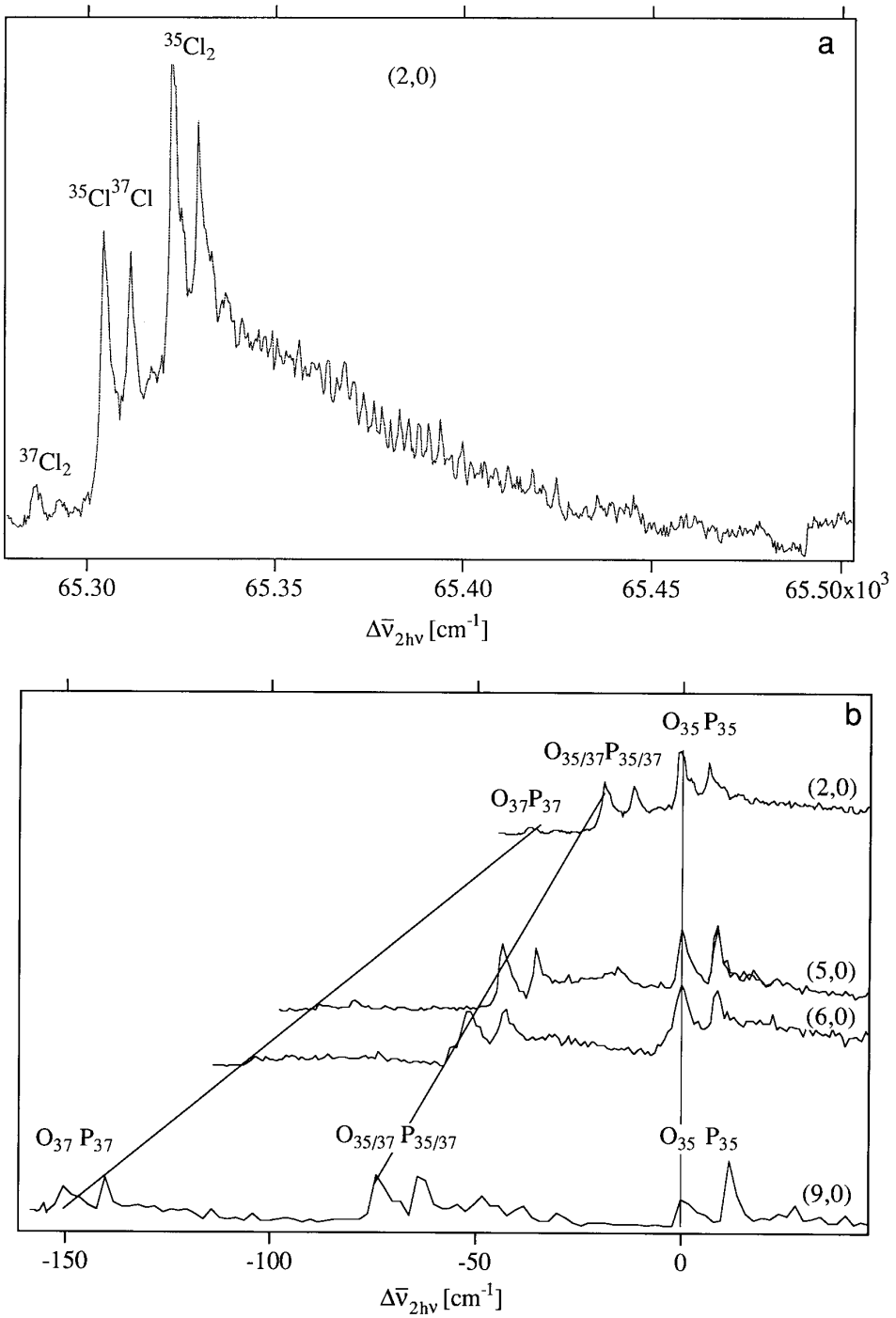

FIG. 1. (2 + 1) REMPI (a) rotational contour/(2, 0) vibrational band and (b) bandheads (v', 0); $v' = 2, 5, 6, 9$ for the $2^1\Pi_g \leftarrow X$ resonance transition for $^{35}Cl_2$, $^{35}Cl^{37}Cl$, and $^{37}Cl_2$: relative intensities versus two-photon energies (a) and relative two-photon energies (b) (in wavenumbers). (v', 0) assignments and *O* and *P* bandheads for all isotopomers (O_i, P_i) are indicated.

positions ($\bar{\nu}(i, O)$) for all isotopomers are listed in Table 1 along with the differences in absolute *O*-peak positions between different isotopomers (ΔO_{ij}) and the differences in absolute positions of *O* and *P* peaks for each bandhead, $\Delta(OP)$. Characteristically the spacing between bandheads for different isotopomers increases with vibrational quantum number for the Rydberg state, v', and $\Delta(OP)$ increases as v' increases (for $v'' = 0$), indicating a decreasing $B_{v'}$ as v' increases (*19*) (see Table 1 and Fig. 1b).

The blue degradation of the vibrational bands indicates

TABLE 1

***O* Bandhead Positions ($\bar{\nu}(i, O)$) (a), Differences between *O* Bandheads within Each Vibrational Band (ΔO_{ij}) (b), and Spacings between *O* and *P* Bandheads (c) for (v', v'' = 0) Bands in the $2^1\Pi_g \leftarrow X$ (2 + 1) REMPI Spectrum for Cl_2 Isotopomers**

(a) $\bar{\nu}$(i,O) (i= 35,35/37, 37) (cm^{-1})[a]

(v´,v´´)	$\bar{\nu}$(35,O)	$\bar{\nu}$(35/37,O)	$\bar{\nu}$(37,O)
(0,0)	64023.2	64023.2	64023.2
(2,0)	65322.8	65304.4	65286.8
(5,0)	67258.0	67214.0	67170.0
(6,0)	67893.6	67842.4	67789.6
(8,0)	69134.0		
(9,0)	69755.6	69680.4	69603.6

(b) ΔO_{ij} (cm^{-1})

(v´,v´´)	$\Delta O_{35,35/37}$	$\Delta O_{35,37}$	$\Delta O_{35/37,37}$
(0,0)	0.0	0.0	0.0
(2,0)	18.4	36.0	17.6
(5,0)	44.0	88.0	44.0
(6,0)	51.2	104.0	52.8
(9,0)	75.2	152.0	76.8

(c) Wavenumber differences between O and P heads (Δ(OP)) for Cl_2 isotopomers

(v´,v´´)	Δ(OP)(i=35)	Δ(OP)(i=35/37)	Δ(OP)(i=37)
(0,0)	5.2±0.3	5.2±0.3	5.2±0.3
(2,0)	7.0±0.3	7.2±0.3	6.2±0.3
(5,0)	8.0±0.6	8.0±0.6	8.0±0.6
(6,0)	8.8±0.6	8.8±0.6	8.8±0.6
(8,0)	10.2±0.6		
(9,0)	12.0±0.6	11.2±0.6	10.4±0.6

[a] Average absolute errors are ± 2.0 cm^{-1}.

that the average internuclear distances between the nuclei are shorter in the Rydberg state than in the ground state. Each vibrational band consists of overlapping rotational line series *O*, *P*, (*Q*), *R*, and *S* for all isotopomers, *Q* being negligible, however (*19*). The lines are too congested to be fully resolved, but fine oscillatory structure due to a favorable overlap of rotational lines can be observed in the band tails (Fig. 1a) (see also below).

(b) Calculated Spectra

Simulations of the vibrational bands (v', 0) for all three isotopomers, $^{35}Cl_2$, $^{35}Cl^{37}Cl$, and $^{37}Cl_2$, were performed in order to obtain rotational constants ($B_{v'}$ and $D_{v'}$) as well as vibrational spectroscopic parameters for the $2^1\Pi_g$ Rydberg state.

The simulations involved calculations of resonance frequencies and relative intensities for all rotational transitions of concern. The procedure has been described elsewhere for one isotopomer (*18, 19*) (I_2) and two isotopomers (*21*) (iodine bromide, $I^{79}Br$ and $I^{81}Br$).

The wavenumber position of a rotational line due to the transition $2^1\Pi_g(J', v') \leftarrow X(J'', v'')$ for isotopomer *i* is given by

$$\bar{\nu}(i;\ J', v' \leftarrow J'', v'') = \bar{\nu}^0(i; v', v'') + \Delta\bar{E}(i;\ J',\ J''), \quad [8]$$

where $\Delta\bar{E}(i;\ J',\ J'')$ is the difference in rotational energies (in cm^{-1}) for the two states

$$\Delta\bar{E}(i;\ J',\ J'') = (J + \Delta J)(J + \Delta J + 1)\bar{B}_{v'}(i) - (J + \Delta J)^2(J + \Delta J + 1)^2\bar{D}_{v'}(i) - J(J + 1)\bar{B}_{v''}(i) + J^2(J + 1)^2\bar{D}_{v''}(i). \quad [9]$$

$\bar{B}_{v'}(i)$, $\bar{D}_{v'}(i)$ and $\bar{B}_{v''}(i)$, $\bar{D}_{v''}(i)$ are the rotational constants for the isotopomer *i*. $J = J''$ and $\Delta J\ (= J' - J'')$ is −2, −1, 0, +1, and +2 for the *O*, *P*, *Q*, *R*, and *S* series, respectively. Calculated spectra were plotted against relative frequency ($\Delta\bar{\nu}$), defined as

$$\Delta\bar{\nu}(35;\ J',\ J'') = \Delta\bar{E}(35;\ J',\ J'') \quad [10]$$

$$\Delta\bar{\nu}(35/37;\ J',\ J'') = \Delta\bar{\nu}^0(35/37,\ 35) + \Delta\bar{E}(35/37;\ J',\ J'') \quad [11]$$

$$\Delta\bar{\nu}(37;\ J',\ J'') = \Delta\bar{\nu}^0(37,\ 35) + \Delta\bar{E}(37;\ J',\ J''), \quad [12]$$

for all isotopomers. Equations [10] – [12] correspond to setting the band origin for $^{35}Cl_2$ to zero.

The ground state rotational constants for $^{35}Cl_2$, $\bar{B}_{v''}(35)$ and $\bar{D}_{v''}(35)$ for $v'' = 0$, were evaluated from

$$\bar{B}_v = \bar{B}_e - \alpha_e(v + \tfrac{1}{2}) \quad [13]$$

$$\bar{D}_v = \frac{4\bar{B}_v^3}{\omega_e^2} \quad [14]$$

for $v = v''$, based on the $\bar{B}_e$, α_e, and ω_e values listed by Hüber and Herzberg (*24*). These values are listed in Table

TABLE 2

Rotational and Vibrational Spectroscopic Parameters for the Ground Electronic State of $^{35}Cl_2$ Used in the Spectral Analyses

$\bar{B}_e$"[a] / cm^{-1}	0.24399
α_e"[a] / cm^{-1}	0.00149
r_e"[a] / Å	1.9879
$\bar{B}_{v"=0}$[b] / cm^{-1}	0.24325
$\bar{D}_{v"=0}$[c] / cm^{-1}	1.8376 x 10^{-7}
ω_e"[a] / cm^{-1}	559,72
$\omega_e x_e$"[a] / cm^{-1}	2.675
μ / g mol^{-1}	17.4844

[a] From reference 24.
[b] $\bar{B}_{v"}$ evaluated from eq. 13
[c] $\bar{D}_{v"}$ evaluated from eq. 14

2 along with other relevant ground state spectroscopic constants for the isotopomer $^{35}Cl_2$ used in the simulation. The ground state rotational constants for the other isotopomers, 35/37($^{35}Cl^{37}Cl$) and 37($^{37}Cl_2$), were calculated from (*21, 25*)

$$\bar{B}_v(i) = \bar{B}_v(35)\rho^2(i, 35) \qquad [15]$$

$$\bar{D}_v(i) = \bar{D}_v(35)\rho^4(i, 35) \qquad [16]$$

for $i = 35/37, 37$, $v = v''$, while the ground state vibrational parameters for the other isotopomers were calculated from [2] and [3].

Relative line intensities, I_{rel}, for $J', v' \leftarrow J'', v''$ transitions were calculated from

$$I_{rel}(i) = C_{v',v''}a(i)g_N(i;\ J'')S_{J',J''} \times \exp\left(-\bar{E}_{J''}(i)\frac{hc}{kT}\right), \qquad [17]$$

where $\bar{E}_{J''}(i)$ is the rotational energy of rotational level J'' of isotopomer i. $S_{J',J''}$ is the two-photon transition strength depending only on J' and J'' as derived by Bray and Hochstrasser for $\Delta\Omega = 1$ transitions (*26*). $a(i)$ is the percentage natural abundance of isotopomer i (see above). $g_N(i;\ J'')$ is the nuclear statistics factor (*19*). It represents the relative weight of odd (antisymmetric nuclear spin wavefunctions) and even (symmetric nuclear spin wavefunctions) quantum levels in the ground state for the homonuclear isotopomers, $i = 35$ and 37, but is not applicable for the heteronuclear, 35/37 isotopomer which has nonsymmetric nuclear spin wavefunctions. Both ^{35}Cl and ^{37}Cl nuclei are fermions with nuclear spin quantum numbers 3/2; hence the relative degeneracy equals odd J'': even $J'' = 5/3$ (*25*). $C_{v',v''}$ is a constant independent of J' and J'' but depends on the Franck–Condon factor for the $v' \leftarrow v''$ transition and factors such as possible variations in the efficiency of the photoionization, laser power, and geometrical factor (*19*). Temperature (T) was assumed to be 298 K. Finally, all rotational lines were displayed as Gaussian-shaped functions for a chosen bandwidth assumed to be the same for all rotational lines in the same vibrational band.

Figure 2a shows a calculated spectrum for the same parameters as obtained by simulation of the (2, 0) band as well as the individual vibrational bands for each isotopomer 35, 37/37, and 37. Rotational lines are also shown plotted underneath each spectrum. Figure 2b shows the calculations for the narrow region indicated in Fig. 2a. The ''rotational peaks'' in the band tail are due to the overlap of rotational lines which belong to the O, P, R, and S series (Q being negligible) of all isotopomers. The alteration in relative intensities and bandwidths of neighbor ''rotational peaks'' is found to be determined by the degree of overlap of rotational lines.

(c) Simulation Procedure

The simulation calculations were performed via a recurrence type procedure to derive the rotational and vibrational parameters for the Rydberg states. Initially first approximation values for vibrational and rotational parameters were evaluated. The vibrational parameters for $^{35}Cl_2$, $\omega'_e(35)$ and $\omega_e x'_e(35)$, were estimated in a standard way from the spacings between the O and P peaks for the $^{35}Cl_2$ vibrational bands. The rotational parameters $\bar{B}_{v'}(35)$ were estimated from $\Delta(OP)$ for $^{35}Cl_2$ and $B_{v''=0}(35)$ (*27*),

$$\bar{B}_{v'} = \frac{\Delta(OP)\bar{B}_{v''}}{\Delta(OP) - 3\bar{B}_{v''}}, \qquad [18]$$

after which $\bar{D}_{v'}(35)$ could be evaluated by Eq. [14]. (i) The calculated spectra were adjusted by varying $\bar{B}_{v'}(35)$ and $\bar{D}_{v'}(35)$ until best fits of calculated and experimental bandheads and/or rotational contours were obtained. (ii) Band origins for all isotopomers 35, 35/37, and 37 in all vibrational bands were evaluated by comparison of the calculated and experimental spectra. (iii) Finally, the parameters T'_e, $\omega'_e(35)$, and $\omega_e x'_e(35)$ were reevaluated by least-squares fit analysis of all band origins (different v' levels and different isotopomers) based on Eq. [1], assuming the standard relationship between spectroscopic parameters for different isotopomers to be valid (Eqs. [2], [3], [15], and [16]). Steps (i)–(iii) were repeated until insignificant changes in the spectroscopic parameters ($\bar{B}_{v'}(35)$ ($\bar{D}_{v'}(35)$), $\omega'_e(35)$, and $\omega_e x'_e(35)$) were obtained between iterations.

Figure 3a shows the simulation for the (2, 0) band contour, while Fig. 3b shows the simulation for the bandheads (v', 0); $v' = 2, 5, 6, 9$. The analysis resulted in evaluations

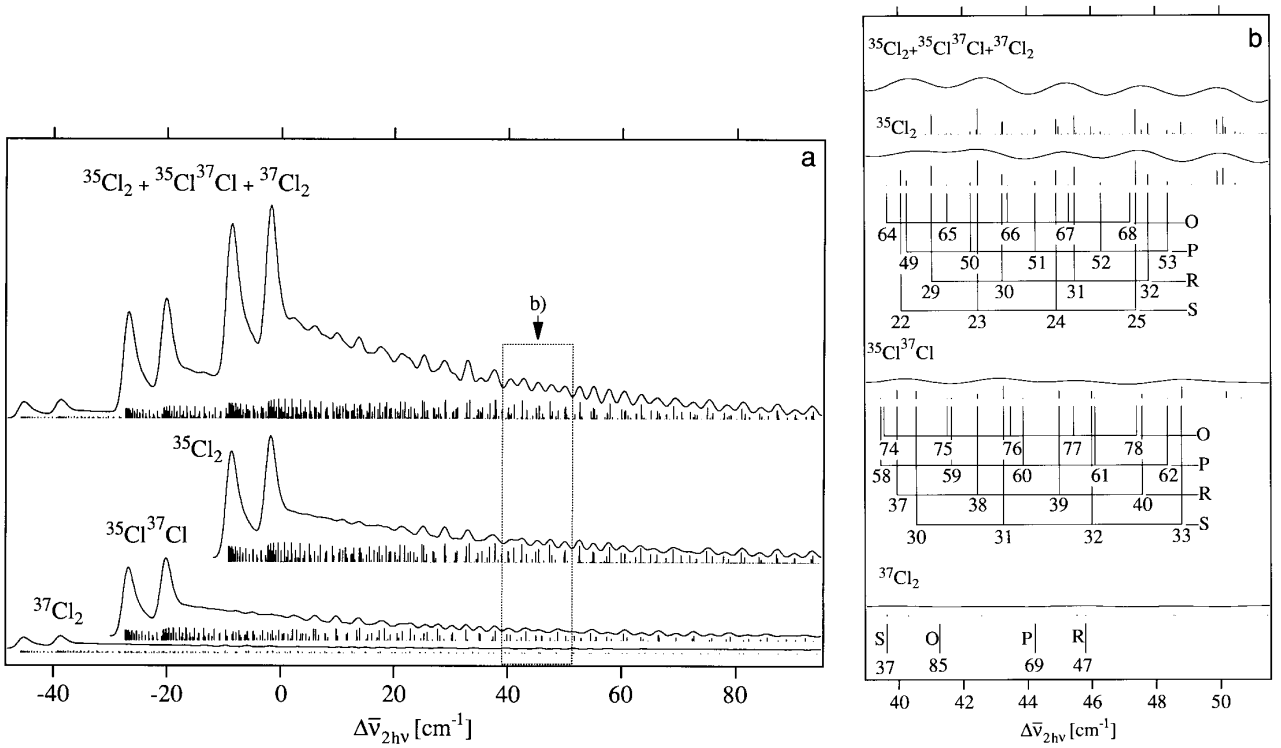

FIG. 2. Calculated rotational contour and rotational lines for a (2 + 1) REMPI vibrational band (v', v'') in the relative wavenumber scale ($\Delta\bar{\nu}_{2h\nu}$) regions from −48 to +92 cm^{-1} (a) and +39 to +51 cm^{-1} (b) for $^{37}Cl_2$ (bottom), $^{35}Cl^{37}Cl$, $^{35}Cl_2$, and isotopomer natural abundance mixture (top). Boltzmann distribution for 25°C is assumed. Rotational constants (B', D', B'', and D'') corresponding to $v' = 2$ and $v'' = 0$ and vibrational parameters (ω_e', $\omega_e x_e'$, ω_e'', and $\omega_e x_e''$) in Tables 2 and 4 were used. Bandwidth of rotational lines is 0.9 cm^{-1} (on the $2h\nu$ scale). The x axis scale ($\Delta\bar{\nu}_{2h\nu}$) equals $\Delta\bar{\nu}(i, J', J'')$ as defined by Eqs. [10]–[12]. Rotational line numbers in (b) are J''.

of band origins, listed in Table 3. Spectroscopic parameters for the Rydberg state $2\,^1\Pi_g$ of molecular chlorine, obtained from the simulation calculations, are listed in Table 4. These values are for isotopomer $^{35}Cl_2$. The spectroscopic parameters $\bar{B}_e'$ and α_e' were obtained from a least-squares fit analysis based on Eq. [13]. Average internuclear distance values, $r_{v'}$

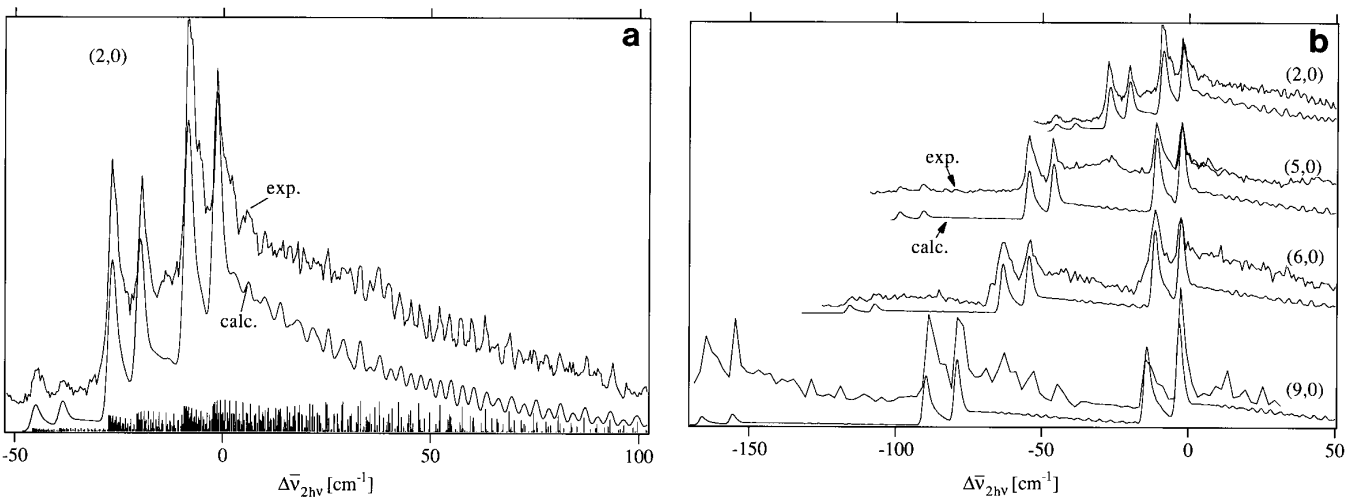

FIG. 3. Simulation of (2 + 1) REMPI vibrational contours for the $2\,^1\Pi_g \leftarrow X$ resonance transitions for $^{35}Cl_2$, $^{35}Cl^{37}Cl$, and $^{37}Cl_2$: Rotational contour for the (2, 0) band (a) and bandheads for (v', 0); $v' = 2, 5, 6, 9$ (b). Bandwidth of rotational lines in the simulation of the (2, 0) band (a) is 0.9 cm^{-1}. See spectroscopic parameters in Tables 2 and 4.

TABLE 3
Vibrational Band Origins ($\bar{\nu}^0(i, v', v'')$) in cm^{-1} for $^{35}Cl_2$, $^{35}Cl^{37}Cl$, and $^{37}Cl_2$ (i.e., i = 35, 35/37, 37)

(v´,v´´)	$\bar{\nu}$o((35,v´,v´´)	$\bar{\nu}$o((35/37,v´,v´´)	$\bar{\nu}$o((37,v´,v´´)
(0,0)	64030.2	64030.2	64030.2
(2,0)	65331.5	65312.8	65295.0
(5,0)	67269.0	67224.7	67180.2
(6,0)	67905.1	67853.6	67800.4
(8,0)	69146.6		
(9,0)	69769.6	69694.2	69617.0

and r_e, were evaluated according to the rigid rotor approximation.

(d) Discussion

Spectroscopic parameters for the $2^1\Pi_g$ state have been reported for $^{35}Cl_2$ by Koenders *et al.* (*8*). The vibrational parameters are based on analysis of bandheads of REMPI–PES spectra for $^{35}Cl_2$. The rotational parameters are based on analysis of bandhead shapes of two vibrational bands, the (2, 0) and (5, 0) bands, for the $^{35}Cl_2$ isotopomer as described before (see Table 4b). Band positions derived from bandhead positions of (2 + 1) REMPI spectra obtained by ion mass detection have been given by Al-Kahali *et al.* (*1*) and Li *et al.* (*10*). For comparison we evaluated ω_e and $\omega_e x_e$ values from these data (see Table 4b). Both the band positions and the vibrational parameters are in reasonable agreement with our results, bearing in mind the nature of the difference in analysis methods, but our results are based on determination of band origins and simulations of band contours and/or bandheads of vibrational bands of all three isotopomers $^{35}Cl_2$, $^{35}Cl^{37}Cl$, and $^{37}Cl_2$ for $v' \leqslant 9$ as described above.

The slightly higher anharmonicity values derived from the bandhead analysis ($\omega_e x_e \sim 2.9-3.2$ cm^{-1} compared to 2.62 cm^{-1}) could be due to the fact that the difference between bandhead peaks (*O* or *P* heads) and band origins is v' dependent. We recalculated all vibrational bands (v', 0) for $v' = 0-19$ and found out that the strongest *P* bandheads approach the band origin as v' increases, which would result in overestimation of $\omega_e x_e$ values for a vibrational analysis based on position of *P* bandheads. Our anharmonicity constant closely resembles that for the ground state ($\omega_e x_e$ ($^{35}Cl_2(X)$) = 2.675 cm^{-1} (*24*)), while the vibrational frequency is about 18.7% larger than that for the ground state (559.72 cm^{-1}). Both values closely resemble those for the ground ionic state ($\omega_e(Cl_2^+) \sim 645$ cm^{-1} and $\omega_e x_e(^{35}Cl_2^+(X)) \sim 3$ cm^{-1} (*28*)), however.

The rate of change in the rotational constants $B_{v'}$ with v', determined by α_e, closely resembles that for the ground state ($\alpha_e(^{35}Cl_2) = 1.49 \times 10^{-3}$ cm^{-1}) (*24*).

As pointed out before (*10*), even though the $2^1\Pi_g$ state has been predicted to mix homogeneously with an ion pair state to form an adiabatic double-well potential (*16*), the regularity in the vibrational progression and rotational structure indicates virtually unperturbed Rydberg character, suggesting that a diabatic approximation indeed is more appropriate.

The (2, 0) band is the most intense band in the vibrational progression. It has been suggested that its large intensity is due to an interaction with the repulsive valence state $^1\Pi_{1g}$, which has been predicted to cross the $2^1\Pi_g$ state near its energy minimum to cause predissociation followed by Cl atom ionization (*1*). While predissociation could explain to some extent the large bandwidths of rovibrational levels which were observed (*1*), we believe that laser power broadening also needs to be considered. The large intensity of the (2, 0) band allowed us to record its rotational contour at low laser power and thus to reduce power broadening significantly. Nevertheless, under such conditions rotational linewidths were found to be as high as 0.9 cm^{-1} (on the $2h\nu$ scale; see Figs. 2 and 3).

TABLE 4
Spectroscopic Parameters for the $2^1\Pi_g$ Rydberg State of $^{35}Cl_2$

(a) Rotational constants ($\bar{B}_{v'}$(35) and $\bar{D}_{v'}$(35)) and internuclear distances, $r_{v'}$, for vibrational states v´ of 2 $^1\Pi_g$ derived from our analysis of (v',v") bands

(v´,v´´)	$\bar{B}_{v'}$(35)/cm^{-1}	$\bar{D}_{v'}$(35)/cm^{-1}	$r_{v'}$/Å
(0,0)	0.282±0.003	1 x 10^{-6}	1.85±0.02
(2,0)	0.2730±0.0014	1.05 x 10^{-6}	1.879±0.010
(5,0)	0.267±0.002	1 x 10^{-6}	1.90±0.01
(6,0)	0.266±0.002	1 x 10^{-6}	1.90±0.01
(8,0)	0.263±0.001	1 x 10^{-6}	1.91±0.01
(9,0)	0.262±0.001	1 x 10^{-6}	1.92±0.01

(b) Equilibrium rotational, vibrational and electronic parameters for $2\ ^1\Pi_g$

	this work [a]	from ref. 10 [b]	from ref. 8	from ref. 1 [c]
B_e'/ cm^{-1}	0.2763±0.0008		0.284±0.002	
α_e' / cm^{-1}	(1.5±0.1) x 10^{-3}		3.3 x 10^{-3}	
r_e' / Å	1.868±0.005		1.84±0.04	
D_e' / cm^{-1}	1 x 10^{-6}			
ω_e' / cm^{-1}	664.8±0.2	673	~660	668
$\omega_e x_e'$ / cm^{-1}	2.62±0.02	3.2	~3	2.9
T_e / cm^{-1}	63970±3	63960		

[a] uncertainty limits are based on standard errors from least squares fit analysis as well as errors introduced by the measurement uncertainties on the O and P band head separations, given in Table 1.
[b] evaluated from data in ref. 10, table I, by least square fit analysis.
[c] evaluated from data in ref. 1, table II, by least square fit analysis.

CONCLUSIONS

Simulation calculations of the rotational contours and bandheads of the (2 + 1) REMPI spectrum of Cl_2 at room temperature (natural abundance of $^{35}Cl_2$, $^{35}Cl^{37}Cl$, and $^{37}Cl_2$ isotopomers) due to the resonance transition $2^1\Pi_g \leftarrow X^1\Sigma_g^+$ have been performed. The spectra were analyzed by assuming that the energies of the rotational levels involved can be formulated in the simple form $\bar{E}(J) = \bar{B}J(J+1) - \bar{D}J^2(J+1)^2$ and by using explicit forms of linestrengths determined by Bray and Hochstrasser (*26*) for $\Delta\Omega = 1$ transitions for excitation by a linearly polarized light. Analogous spectroscopic parameters for different isotopomers ($^iCl_2$ and $^jCl_2$) were assumed to be related by the expression $\beta(^iCl_2) = \beta(^jCl_2)\rho^n(\beta = \omega_e, \omega_e x_e, B, D$; see Eqs. [2], [3], [15], and [16] for ρ and n). The analysis allowed evaluation of rotational constants, internuclear distances, band origins, and vibrational and electronic parameters for the $2^1\Pi_g$ Rydberg state to make it the best characterized high-lying Rydberg state for Cl_2 at present.

ACKNOWLEDGMENTS

We are grateful for financial support from the Icelandic Science Foundation, the University of Iceland Research Fund, and The Icelandic Research Fund for Higher Education. We thank Professor R. J. Donovan and coworkers for making new results available to us prior to publication.

REFERENCES

1. M. S. N. Al-Kahali, R. J. Donovan, K. P. Lawley, Z. Min, and T. Ridley, *J. Chem. Phys.* **104,** 1825–1832 (1996).
2. M. S. N. Al-Kahali, R. J. Donovan, K. P. Lawley, and T. Ridley, *J. Chem. Phys.* **104,** 1833–1838 (1996).
3. M. S. N. Al-Kahali, R. J. Donovan, K. P. Lawley, T. Ridley, and A. J. Yarwood, *J. Phys. Chem.* **99,** 3978–3983 (1995).
4. P. Wang, S. S. Dimov, G. Rosenblood, and R. H. Lipson, *J. Phys. Chem.* **99,** 3984–3989 (1995).
5. P. Wang, I. V. Okuda, S. S. Dimov, and R. H. Lipson, *Chem. Phys. Lett.* **229,** 370–376 (1994).
6. T. Ishiwata, J.-h. Si, and K. Obi, *J. Chem. Phys.* **96,** 5678–5686 (1992).
7. T. Tsuchizawa, K. Yamanouchi, and S. Tsuchiya, *J. Chem. Phys.* **93,** 111–120 (1990).
8. B. G. Koenders, S. M. Koeckhoven, G. J. Kuik, K. E. Drabe, and C. A. deLange, *J. Chem. Phys.* **91,** 6042–6051 (1989).
9. B. G. Koenders, D. M. Wieringa, G. J. Kuik, K. E. Drabe, and C. A. D. Lange, *Chem. Phys.* **129,** 41–50 (1989).
10. L. Li, R. J. Lipert, H. Park, W. A. Chupka, and S. D. Colson, *J. Chem. Phys.* **88,** 4608–4613 (1988).
11. J. Wörmer, T. Möller, J. Stapelfeldt, G. Zimmerer, D. Haaks, S. Kampf, J. L. Calvé, and M. C. Castex, *Z. Phys. D Atoms, Molecules Clusters* **7,** 383–395 (1988).
12. B. G. Koenders, D. M. Wieringa, K. E. Drabe, and C. A. D. Lange, *Chem. Phys.* **118,** 113–121 (1987).
13. L. Li, R. J. Lipert, H. Park, W. A. Chupka, and S. D. Colson, *J. Chem. Phys.* **87,** 6767–6769 (1987).
14. L. C. Lee, M. Suto, and K. Y. Tang, *J. Chem. Phys.* **84,** 5277–5283 (1986).
15. T. Shinzawa, A. Tokunaga, T. Ishiwata, and I. Tanaka, *J. Chem. Phys.* **83,** 5407–5412 (1985).
16. S. D. Peyerimhoff, and R. J. Buenker, *Chem. Phys.* **57,** 279–296 (1981).
17. A. E. Douglas, *Can. J. Phys.* **59,** 835 (1981).
18. W. Huasheng, J. Ásgeirsson, Á. Kvaran, R. J. Donovan, R. V. Flood, K. P. Lawley, T. Ridley, and A. J. Yencha, *J. Mol. Struct.* **293,** 217–222 (1993).
19. Á. Kvaran, H. Wang, and J. Ásgeirsson, *J. Mol. Spectrosc.* **163,** 541–558 (1994).
20. R. J. Donovan, R. V. Flood, K. P. Lawley, A. J. Yencha, and T. Ridley, *Chem. Phys.* **164,** 439–450 (1992).
21. Á. Kvaran, H. Wang, and G. H. Jóhannesson, *J. Phys. Chem.* **99,** 4451–4457 (1995).
22. J. Jureta, S. Cvejanovic, M. Kurepa, and D. Cvejanovic, *Z. Phys. A* **304,** 143 (1982).
23. D. Spence, R. H. Huebner, H. Tanaka, M. A. Dillon, and R.-G. Wang, *J. Chem. Phys.* **80,** 2989–2996 (1984).
24. K. P. Hüber, and G. Herzberg, ''Constants of Diatomic Molecules.'' Van Nostrand–Reinhold, New York, 1979.
25. G. Herzberg, ''Molecular Spectra and Molecular Structure. I. Spectra of Diatomic Molecules,'' 2nd ed., p. 658. Van Nostrand–Reinhold, New York, 1950.
26. R. G. Bray, and R. M. Hochstrasser, *Molec. Phys.* **31,** 1199–1211 (1976).
27. Á. Kvaran, H. Wang, G. H. Jóhannesson, and A. J. Yencha, *Chem. Phys. Lett.* **222,** 436–442 (1994).
28. H. v. Lonkhuyzen, and C. A. DeLange, *Chem. Phys.* **89,** 313–322 (1984).